Trans. Phenom. Nano Micro Scales, 5(2): 85-96, Summer and Autumn 2017
DOI: 10.7508/tpnms.2017.02.002

ORIGINAL RESEARCH PAPER

Synthesis and characterization of magnetic γ- Fe_2O_3 nanoparticles: Thermal cooling enhancement in a sinusoidal headbox

Mohammad Soleimani Lashkenari[1], Mazaher Rahimi-Esbo[2,], Mohsen Ghorbani[3], Amin Taheri[4], Shokoofeh Ghasemi[5]*

[1]*Amol University of Special Modern Technologies, Amol 46168-49767, Iran*
[2]*Faculty of Mechanical Engineering, Malek Ashtar University of Technology, Freydounkenar, Iran*
[3]*Department of Chemical Engineering, Babol University of Technology, P.O.Box 484, Babol, Iran*
[4]*School of Mechanical Engineering, Mazandaran University of Science and Technology, Babol, Iran*
[5]*Faculty of Chemical, Gas and Petroleum Engineering, Semnan University, Semnan, 35131-19111, Iran*

Received 21 January 2016; revised 22 May 2016; accepted 11 November 2016; available online 10 June 2017

ABSTRACT: Nano-size maghemite (γ-Fe_2O_3) particles were prepared in one step using ultrasound radiation. The obtained nanoparticles were characterized by SEM, TEM , XRD, FTIR, and VSM. The results revealed that the synthesized nanoparticles were spherical, mono-dispersed and uniform. Furthermore, the crystalline structure of nanoparticles endorsed by X-ray diffraction study. The FTIR spectra have provided information on the structure of the surface of nanoparticles. TEM analysis showed that the average particle size of the γ -Fe_2O_3 are about 15 nm. The formed nanoparticles exhibited unique magnetic behavior with magnetic saturation values of ~68 emu/g. By utilizing properties of synthetic γ -Fe_2O_3 nanoparticles, a three-dimensional incompressible nanofluid flow in a confined sinusoidal converging jet in turbulent flow regime was numerically investigated. Results were obtained for the flow structure at different Reynolds numbers for steady asymmetric jet development at various values of the duct-to-jet width ratio (aspect ratio), different amplitudes and different volume fractions of nanoparticles. The results showed that by increasing the Reynolds number, aspect ratio, amplitude and volume fraction of γ -Fe_2O_3 nanoparticles, the averaged Nusselt number will increase.

KEYWORDS: *Maghemite, γ-Fe_2O_3; Nanoparticle;Headbox; Heat transfer*

INTRODUCTION

Nanoparticles have become the focus of modern materials science because of their potential technological importance, which stems from their unique physical properties [1]. In recent years, metal oxide nanoparticles have attracted substantial interest because of their unique optical, magnetic and electronic properties [2,3]. These properties hold promises for remarkable performance in several important fields of application, including catalytic, magnetic, medicine [4], mechanical and biological applications [5].Among various transitions metal oxides, maghemite is the most stable iron oxide, low-cost and high resistance to corrosion, which is extensively used as catalysts, gas sensors, anti-corrosive agents, fine ceramics, data storage materials and pigments, light absorption, medicine, adsorbents in waste-water treatment, bio separation. Furthermore, it is considered to be a potential candidate for possible photo electrochemical cells [6-8].

Fluids with suspended nanoparticles are called nanofluid, a term proposed in 1995 by Choi [9] of the Argonne National Laboratory, USA. Nanofluids can be considered to be the next generation of heat transfer fluids because they offer exciting new possibilities to enhance heat transfer performances compared to pure liquids. They are expected to have superior properties compared to conventional heat transfer fluids, as well as fluids containing micro-sized metallic particles [10]. Experimental studies on the heat transfer characteristics of a flow of nanofluids can guarantee high accuracy. However, besides being expensive, it takes a while. Numerical modeling is more effective and workable that can be done within a shorter time and lower cost compared with the experimental method [11].The headbox is a critical component in the paper making system. The rapidly converging section of a paper machine headbox carries a dilute concentration of pulp fibers to the wire mesh where the fibers are dried to become paper. Rahimi-Esbo et al. [12] numerically studied force convection of turbulent nanofluid flow in a converging duct. Their results show that by increasing the Reynolds number, aspect ratio, and volume fraction the average Nusselt number will increase. Furthermore, they demonstrated in the investigations that increasing the Reynolds number and aspect ratio, the length of the recirculation zones rise. This has a direct impact on the local Nusselt number which, consequently, increases the average Nusselt number.Esmaeili et al. [13] synthesized the porous superparamagneticFe_3O_4 nanoparticles with an average particlesize of 75 nm through a potentialsolvo-

*Corresponding Author Email: *mrahimi@mut.ac.ir*
Tel.: +989116277073; Note. This manuscript was submitted on January21, 2016; approved on May22, 2016; published online June 10, 2017.

Nomenclature

AR	Aspect ratio =(h/d)	V_b	Brownian velocity of nanoparticles (m/s)
$c_1, c_2,$	Constant parameters	u	*Velocity (m/s)*
c_p	Specific heat (kJ/kg.K)		**Greek symbols**
d	Jet length (m)	α	Amplitude of the waves (m)
d_f	Diameter of base fluid molecules (m)	α_f	Thermal diffusivity (m^2/s)
d_p	Average diameter of nanoparticles (m)	δ	Center to center distance of nanoparticles (m)
h	Height of channel(m)	ε	Turbulent dissipation rate
j	Colburnfactor (Nu / (Re $Pr^{1/3}$))	Φ	Volume fraction (%)
K	Thermal conductivity (w/m.k)	λ	wavelength of the waves (m)
k	Turbulent kinetic energy	μ	Viscosity (Pa.s)
k_b	Boltzmann number (J/K)	ρ	Density (kg/m^3)
l_f	Free average distance of water molecules (m)	Γ	Thermal diffusivity
N	Parameter for adapting the results with experimental data		**Subscripts**
n	Direction normal on walls	avg	Average
Nu	Nusselt number	f	Base fluid
P	Pressure (Pa)	in	Inlet
Pr	Prandtl number	nf	Nanofluid
Re	Reynolds number	p	Particle
T	Temperature (K)	t	Turbulent
T_B	Bulk temperature of nanofluid (K)	w	Wall
N	Parameter for adapting the results with experimentaldata		

-thermal method in order to investigate the influence of a 3-D low voltage magnetic field on the convective heat transfer measurements. According to their results, use of the magnetic field had a significant effect on the heat transfer values induced by both Brownian motions and viscosity gradients; however, this enhancement was strongly sensitive to the applied field strength. Conclusively, their findings showed promising insights into the enhancement of the forced-convective heat transfer properties of nanofluids by applying an appropriate magnetic field.

Zeinali et al. [14] experimentally investigated laminar convective heat transfer of CuO/water nanofluid through square cross section cupric duct with constant uniform heat flux boundary conditions.

Experimental results have clearly revealed that the addition of nanoparticles could remarkably increase the heat transfer rate compared to that while using the distilled water (base fluid) alone. Such heat transfer enhancement appeared to be more related to the increase of nanoparticles' volume concentration. They discovered that using nanofluids as a thermal fluid medium can be used as a solution to overcome poor heat transfer performance of non-circular ducts.

In this paper, the single-phase method has been used. Although a twophase flow methods causes higher accuracy in the numerical results, the single-phase method has still been using in recent studies concerned on a computational simulation on nanofluids[15-18].

To the best of author's knowledge, there is no theoretical study in literature reports on the enhancement of heat transfer of γ-Fe_2O_3nanofluids flowing in a headbox. Therefore, it is worthwhile to computationally obtain information about the enhancement of heat transfer of γ-Fe_2O_3 nanofluids flowing in a headbox. In this article, γ-Fe_2O_3 nanoparticles were synthesized in one step using ultrasound radiation and product was investigated in terms of morphology and chemical structure. In the second part, the velocity and temperature distribution, the Nusselt number along both top and bottom walls downstream from the inlet section and the velocity profile at different sections of a paper machine headbox are investigated. Also, the effect of γ-Fe_2O_3 nanoparticles on thermal and flow characteristics and the effect of aspect ratios on flow features and heat transfer properties are investigated.

MATERIALS

The chemical materials used for the fabrication of γ-Fe_2O_3 nanoparticles were Iron(II) chloride tetrahydrate ($FeCl_2.4H_2O$), Iron(III) chloride ($FeCl_3$), ammonium hydroxide (NH_4OH), Ethanol (C_2H_5OH) and Hydrochloric acid (HCl) from Merck Co. All these chemicals were used as received without any further purification. Distilled water was used throughout the experiment.

SYNTHESIS OF γ- Fe_2O_3 NANOPARTICLES

Maghemite nanoparticles were prepared in one step as the following: First, 2 ml of HCl (2 $molL^{-1}$) and 20 ml distilled water were added successively to 5.33 gr $FeCl_2.4H_2o$ under magneticstirring. 6.22 gr $FeCl_3$ was dissolved in 38 ml distilled water with stirring and injected to the former solution and stirred at room temperature for minutes to obtain homogeneous solution. After that, 600 ml of NH_4OH (2 mol L^{-1}) solution was added dropwise into the

above solution in an ultrasonic bath at room temperature. A reddish-brown precipitate quickly formed.
The precipitate was washed with excess distilled water and ethanol until the pH was adjusted to 3.5 which were repeated at least three times and then dried at 40 °C under vacuum oven for 48 hr.

MODEL DESCRIPTION AND MATHEMATICAL FORMULATION

For heat transfer of γ-Fe_2O_3nanofluids flowing in a paper machine headbox, the 3-D incompressible turbulent nanofluid flow is considered. For simplicity, the inlet flow is taken as isothermal, and the velocity profile at the inlet is taken as uniform. The considered geometry and the flow configurations used in this work are shown in Figure 1. The nanoparticles and the base fluid (i.e., water) are assumed to be in thermal equilibrium and no slip condition occurs between them. The other boundary conditions are mentioned in Figure 1.

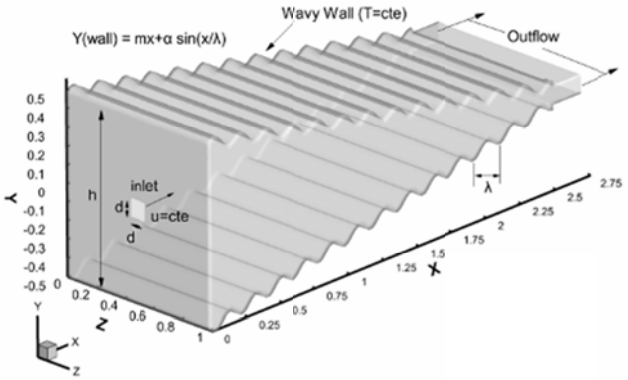


Fig. 1. Geometry and boundary condition of the problem

The aspect ratio is taken as follows:

$$AR = \frac{h}{d} \tag{1}$$

The continuity, momentum, and energy equations for the 3-D flow problem are given by the following:

Continuity

$$\frac{\partial}{\partial x_i}\left(\rho_{nf} u_i\right) = 0 \tag{2}$$

Momentum

$$\rho_{nf}\frac{\partial u_i}{\partial x_j} + \frac{\partial u_i}{\partial x_j}\left(\rho_{nf} u_i u_j\right) = -\frac{\partial p}{\partial x_i} + \frac{\partial}{\partial x_j}\left[\mu\left(\frac{\partial u_i}{\partial x_j} + \frac{\partial u_j}{\partial x_i}\right)\right] + \frac{\partial}{\partial x_j}\left(\rho_{nf}\overline{u_i' u_j'}\right) \tag{3}$$

Energy

$$\rho_{nf}\frac{\partial T}{\partial t} + \frac{\partial}{\partial x_i}\left(\rho_{nf} u_i T\right) = \frac{\partial}{\partial x_j}\left(\left(\Gamma + \Gamma_t\right)\frac{\partial T}{\partial x_j}\right) \tag{4}$$

Where Γ and Γ_t are the molecular thermal diffusivity and turbulent thermal diffusivity, respectively, and are given by the following:

$$\Gamma = \mu_{nf} / Pr_{nf} \quad , \quad \Gamma_t = \mu_t / Pr_t \tag{5}$$

The Reynolds-averaged approach to turbulence modeling requires that the Reynolds stresses, i.e.$\rho_{nf}\overline{u_i' u_j'}$ be modeled. For this purpose the *k–ε* model is chosen. A common method employs the Boussinesq hypothesis to relate the Reynolds stresses to the mean velocity gradients.

$$\rho_{nf}\overline{u_i' u_j'} = \mu_t\left(\frac{\partial \mathrm{u_i}}{\partial \mathrm{x_j}} + \frac{\partial \mathrm{u_j}}{\partial \mathrm{x_i}}\right) \tag{6}$$

The turbulent viscosity term is needed to be computed, which is defined as follows:

$$\mu_t = \rho_{nf} c_\mu k^2 / \varepsilon \tag{7}$$

Following, are transport equations for k and *ε*:

$$\frac{\partial}{\partial t}(\rho k) + \frac{\partial}{\partial x_i}(\rho k u_i) = \frac{\partial}{\partial x_j}\left[\left(\mu + \frac{\mu_t}{\sigma_k}\right)\frac{\partial k}{\partial x_j}\right] + G_k - \rho\varepsilon + S_k \tag{8}$$

and

$$\frac{\partial}{\partial t}(\rho\varepsilon) + \frac{\partial}{\partial x_i}(\rho\varepsilon u_i) = \frac{\partial}{\partial x_j}\left[\left(\mu + \frac{\mu_t}{\sigma_\varepsilon}\right)\frac{\partial \varepsilon}{\partial x_j}\right] + C_{1\varepsilon}\frac{\varepsilon}{k}G_k - C_{2\varepsilon}\rho\frac{\varepsilon^2}{k} + S_\varepsilon \tag{9}$$

Where G_k is the rate of generation of the *TKE*, and ρε is its destruction rate, and is written as follows.

$$G_k = \rho_{nf}\overline{u_i' u_j'}\frac{\partial \mathrm{u_j}}{\partial \mathrm{x_i}} \tag{10}$$

s_k, s_ε are source terms for k and ε and in this research are taken as zero. The boundary values for the turbulent quantities near the wall are specified with the standard wall-treatment method. The values of $c_\mu = 0.009$, $c_{1\varepsilon} = 1.44$, $c_{2\varepsilon} = 1.92$, $\sigma_k = 1.3$, and are $\mathrm{Pr}_t = 0.9$ chosen to be the empirical constants in the turbulent transport equations. The following equations are used to calculate the turbulent intensity (I), turbulent kinetic energy (k), and turbulent dissipation rate (ε) at the inlet section of the headbox[19, 20].

$$I = 0.16 Re^{-1/8} \tag{11}$$

$$k = \left(3/2\right)\left(I \times u_{in}\right)^2 \tag{12}$$

$$\varepsilon = c_\mu^{0.75} \times \left(k^{1.5} / 0.1h \right) \tag{13}$$

The nondimentional flow and heat transfer parameters are defined by the following:

$$Re = \frac{\rho_{nf}\, u\, d}{\mu_{nf}} \tag{14}$$

$$Nu = (K_{nf}\, \partial T / \partial n) / (K_f \left(T_w - T_{in}\right)) \tag{15}$$

$$Nu_{avg} = \frac{\int Nu(x) dx}{L} \tag{16}$$

THERMOPHYSICAL PROPERTIES OF NANOFLUIDhermophysical

Thermal Conductivity

The thermal conductivity of the nanofluid is calculated from Chon et al. [21], which is expressed in the following form:

$$\frac{k_{nf}}{k_f} = 1 + 64.7\, \phi^{0.746} \left(d_f / d_p\right)^{0.369} \times \left(k_p / k_f\right)^{0.7476} \mathrm{Pr}_f^{0.9955}\, \mathrm{Re}_p^{1.2321} \tag{17}$$

$$\mathrm{Re} = \frac{\rho_f k_b T}{3\pi \mu_f^2 \lambda_f}, Pr_f = \mu_f / \rho_f \alpha_f \tag{18}$$

According to average diameter of synthetic γ- Fe_2O_3 nanoparticles (based on the results of Fig. 4), d_p is taken as 15 nm. $k_b$is the Boltzmann constant, 1.3807×10^{-23} and λ_f is the free average distance of water molecules that according to suggestion of Chon et al. is taken as d_f= 0.2 nmλ_f= 0.17 nm. Mintsa et al. [22] approved the accuracy of this model.

Viscosity

The viscosity of the nanofluid is approximated as viscosity of the base fluid $\mu_f$containing dilute suspension of fine spherical particles, as given by Masoumi et al. [23].

$$\frac{\mu_{nf}}{\mu_f} = 1 + \rho_p V_b\, d_p^2 / 72\, N\, \delta \tag{19}$$

$$N = (c_1\phi + c_2) d_p + (c_3\phi + c_4) \tag{20}$$

$$\delta = \sqrt[3]{\frac{\pi}{6\phi}}\, d_p \tag{21}$$

$$V_b = \frac{1}{d_p} \sqrt{\frac{18\, k_b T}{\pi \rho_p d_p}} \tag{22}$$

N is a parameter for adapting the results with experimental data, where C_1=-1.133×e^{-6}, C_2=-2.771×e^{-6}, C_3=9.0×e^{-8}, C_4=-3.93×e^{-7}.

Density and specific heat

The density and specific heat of the nanofluid are calculated by using the Pak and Cho [24] correlations, which are defined as follows.

$$\left(\rho\right)_{nf} = (1-\phi)\rho_f + \phi\rho_p \tag{23}$$

$$C_{p_{nf}} = \frac{(1-\phi)(\rho C_p)_f + \phi(\rho C_p)_p}{\rho_{nf}} \tag{24}$$

$$Pr_f = \mu_{nf} \times c_{p_{nf}} / k_{nf} \tag{25}$$

NUMERICAL PROCEDURE AND VALIDATION

A finite volume technique on a collocated grid is implemented for discretizing the governing equations inside the computational domain. The SIMPLE algorithm is used to link the pressure and velocity fields. For the stability of the solution, the diffusion term in the momentum equations is approximated by the second order central difference scheme. Moreover, a deferred correction scheme is adopted for the convective terms. For turbulent equations, the second order upwind scheme is used for discretizing the convection term. For discretizing, the unsteady term implicit Euler and tree times' level scheme is applied. The Fluent 6.3 software is used for simulation and the nanofluid properties is added to software using user define function(UDF). At the end of any iteration, the residual sum for each of the conserved variables is computed and stored, thus recording the convergence history.

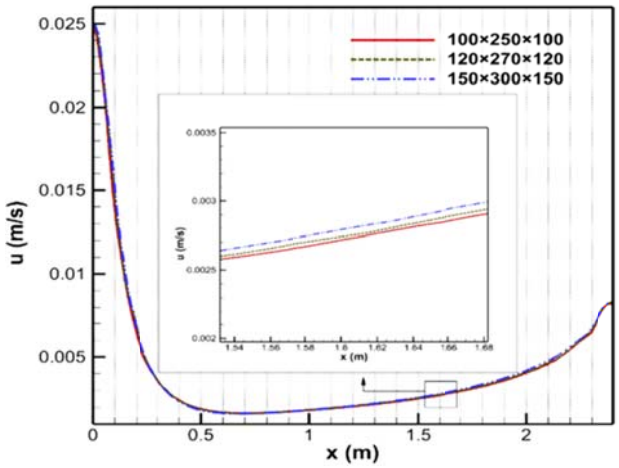


Fig. 2. Midline axial velocity profile for mesh indepency investigation at Re=10,000, AR=5, α = 0.02and ϕ=0%.

The convergence criterion required that the maximum sum of the error for each of the conserved variables be smaller than 1×10^{-3} grid densities of 100×250×100, 120×270×120, and 150×300×150 were selected to perform a grid independency test. Figure 2 shows a less than 1% difference in velocity compared to the chosen grid (150×300×150).

For validation purposes, in Figure 3 Colborn factor(j=Nu / (Re $Pr^{1/3}$)) is compared with numerical result by Pham et al. [25] and experimental data of Zhang et al. [26].

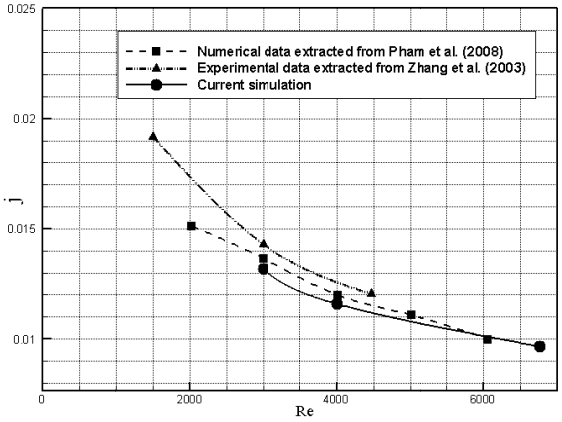
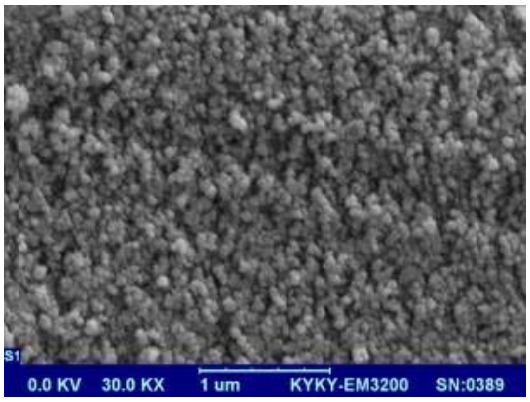


Fig. 3. Global variations of j heat transfer coefficient versus Reynolds numbers for a wavy channel configuration (Colburn factor(Nu / (Re $Pr^{1/3}$)))

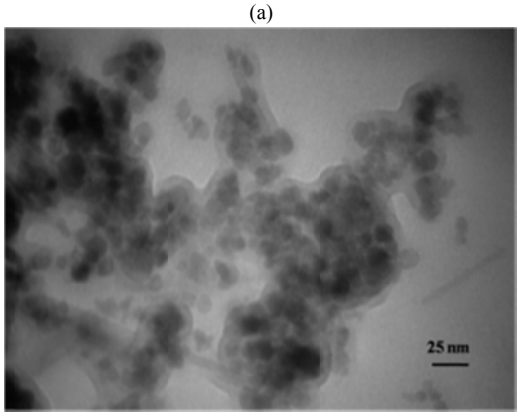
RESULTS AND DISCUSSION

Morphology investigation of γ- Fe_2O_3 nanoparticles

The morphology and nanostructure of the γ- Fe_2O_3 nanoparticles were investigated using transmission electron microscope (TEM; Zeiss-EM10C- Germany) and scanning electron microscope (SEM; KYKY-EM3200-China). Figure (4a) demonstrate that the magnetic nanoparticles synthesized in this study were spherical and monodispersed. From Figure (4b), it can be obviously seen that the synthesized nanoparticles are in nanometer size with the average size about 15 nm.



(a)



(b)

Fig. 4. γ- Fe_2O_3nanoparticles a) SEM and b) TEM image

FTIR spectroscopy of γ- Fe_2O_3 nanoparticles

The chemical composition and structure of samples were analyzed with Fourier–transform infrared spectrophotometer (FTIR; Burker vector 22 spectrometer, Germany) using KBr pellets, in the range of 400 to 4000 cm^{-1}. Figure 5, shows FTIR spectra of the synthesized magnetic nanoparticles.

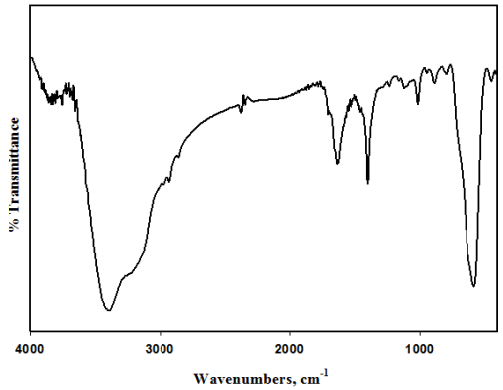


Fig. 5. FTIR spectra of γ-Fe_2O_3 nanoparticles

As displayed in Figure 3, the characteristic vibrations of Fe-O in γ- Fe_2O_3 are clearly observed at 448 and 585 cm^{-1}[27]. In addition, the peak at 1629 cm^{-1} is related to the OH bending of water, and the absorption peak at 3405 cm^{-1} is for the hydroxyl group (–OH) [28]. There is a tiny dip in the spectra at 2368 cm^{-1} due to the presence of atmospheric CO_2[29].

X-ray diffraction of γ- Fe_2O_3 nanoparticles

The crystalline structure of the γ- Fe_2O_3 nanoparticles was characterized by X-ray diffraction (XRD; INEL, EQuinox 3000, France).

The XRD pattern of γ- Fe_2O_3 nanoparticles is shown in Figure 6, which agrees well with the reported data (JCPDS card No. 39-1346). Diffraction peaks at 30.2°, 35.5°, 54.1°, 57.7°and 62.4° are assigned to (220), (311), (422), (511) and (440) crystal planes of γ-Fe_2O_3. The narrow sharp peaks of the XRD pattern indicate that the γ-Fe_2O_3 product was well crystallized [30]. The crystalline size of γ-$Fe_2O_3$was calculated by using Scherrer equation:

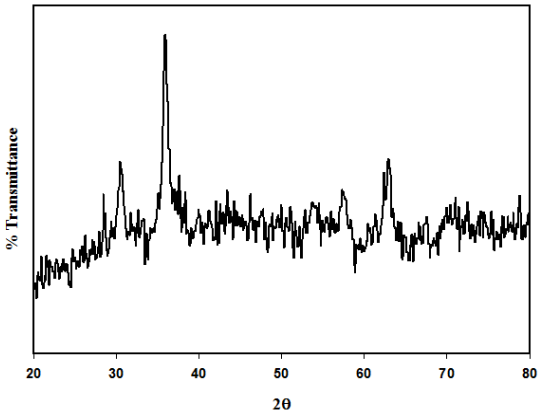


Fig. 6. XRD patterns of γ- Fe_2O_3nanoparticles

$$d = \frac{K\lambda}{\beta \cos\theta} \quad (26)$$

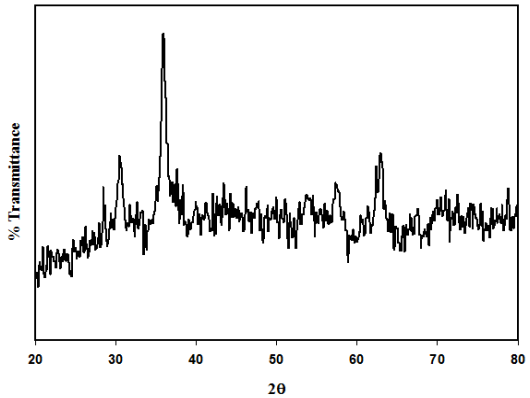


Fig. 6. XRD patterns of γ- Fe_2O_3nanoparticles

Where d is the average crystalline size of the phase under investigation, B is the Scherrer constant (0.89), λ is the wave length of X-ray beam used (λ = 0.154 nm, CuKα), β is the full-width half maximum (FWHM) of diffraction and θ is the Bragg's angle. The crystalline size of γ-$Fe_2O_3$was found to be 20.

Magnetic properties of γ- Fe_2O_3 nanoparticles

The magnetic properties of the γ- Fe_2O_3 nanoparticles were measured using a vibrating sample magnetometer (VSM; meghnatisedaqhiqhkavir, MDK6, Iran). Hematite nanoparticles were dispersed in deionized water by ultrasound (PSA 100-SK1, Korea).

Magnetic properties of γ- Fe_2O_3 nanoparticles were measured at room temperature in applied filed sweeping from +10 to -10 kOe.

As represented in Figure 7 the magnetic hysteresis loops showed S-shaped curves.

Table 1 gives the magnetic parameters such as saturation magnetization (Ms), coercivity (Hc) and remnant magnetization (Mr) that determined by hysteresis loops measurement.

From the Figure 7, it can be seen that the maghemite nanoparticles show ferrimagnetic behavior with magnetic saturation (M_S) value of ~68emu/g.

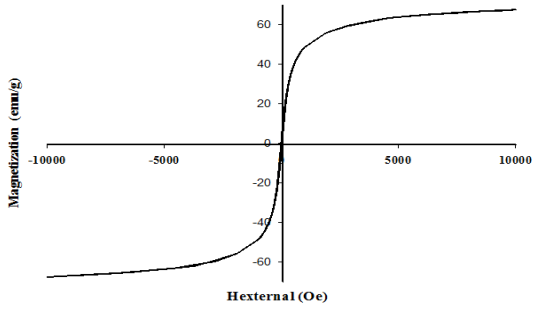


Fig. 7. Magnetic hysteresis loops of γ- Fe_2O_3 nanoparticles

Table 1
VSM results of maghemite nanoparticles.

Hc(A/m)	Mr(emu/g)	Ms(emu/g)	sample
γ- Fe_2O_3	67.7	2.4	17.4

At high Reynolds number and aspect ratio, an asymmetric flow was observed at flow in a converging sinusoidal channel in a steady solution; so, an unsteady solution was seemed to be necessary.

For the case of AR=10, Re=15,000 an unsteady solution is done and the streamline and temperature contours are simultaneously depicted in Figure 8.

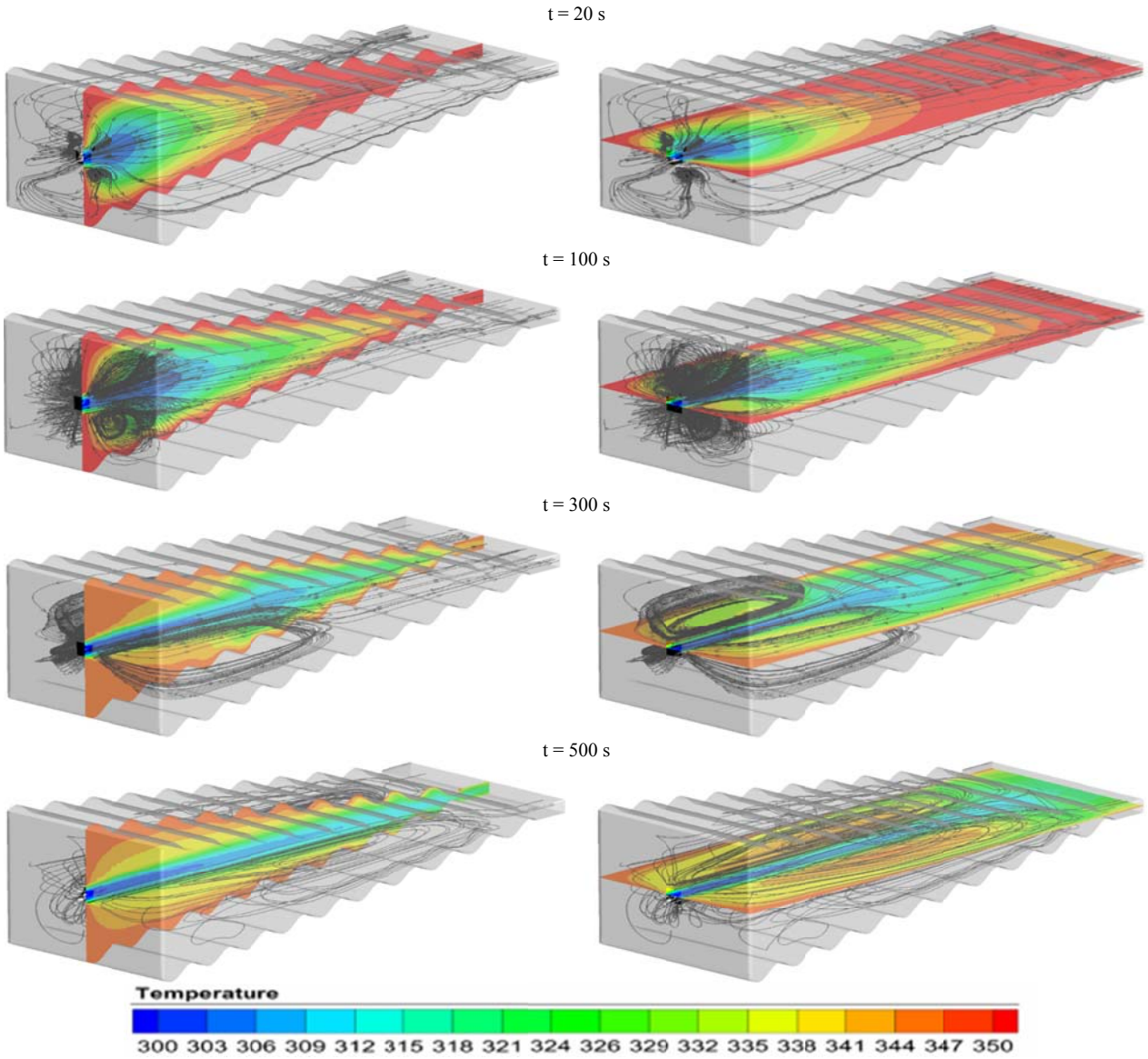


Fig. 8. Streamlines and temperature contours for unsteady solution at AR=20, Re=15,000,α = 0.04 and ϕ=0%

It is observed that after 480 s the streamline remains fixed. According to Figure 8, asymmetric flow occurs for both steady and unsteady cases. It should be noted that the asymmetry in the flow pattern corresponds to a bimodal steady configuration with the jet turning upwards or downwards in a random manner, during any computational run.

Sarma et al. [31] presented this behavior. According to the above proof, the steady solution can be generalized to the unsteady problem. From now on, results are reported on the steady state condition.

In Figure 9 and Figure 10, the steady state streamline patterns at different Reynolds numbers and aspect ratios are depicted. In Figure 9, the effect of Reynolds number on flow structure at AR=10 and ϕ=0% is shown.

It is observed that for a low Reynolds number such as Re=4,000, the jet development is almost symmetric and counter-rotating velocities are seen immediately after the sudden expansion. The jet decay is rapid and the transition from jet-to-duct flow occurs in a short distance. At a higher Reynolds number of Re=10,000, it is observed that the steady state jet flow development is asymmetric. Also, the transition from jet-to-duct flow occurs over a longer distance. For a still higher Reynolds number of 40,000, it is seen that asymmetric flow exhibits a wavy pattern with a larger wavelength and the flow development inside the duct occurs over a larger axial distance. It should be noted that the asymmetry in the flow pattern corresponds to a bimodal steady configuration with the jet turning upwards or downwards in a random manner, during any computational run.

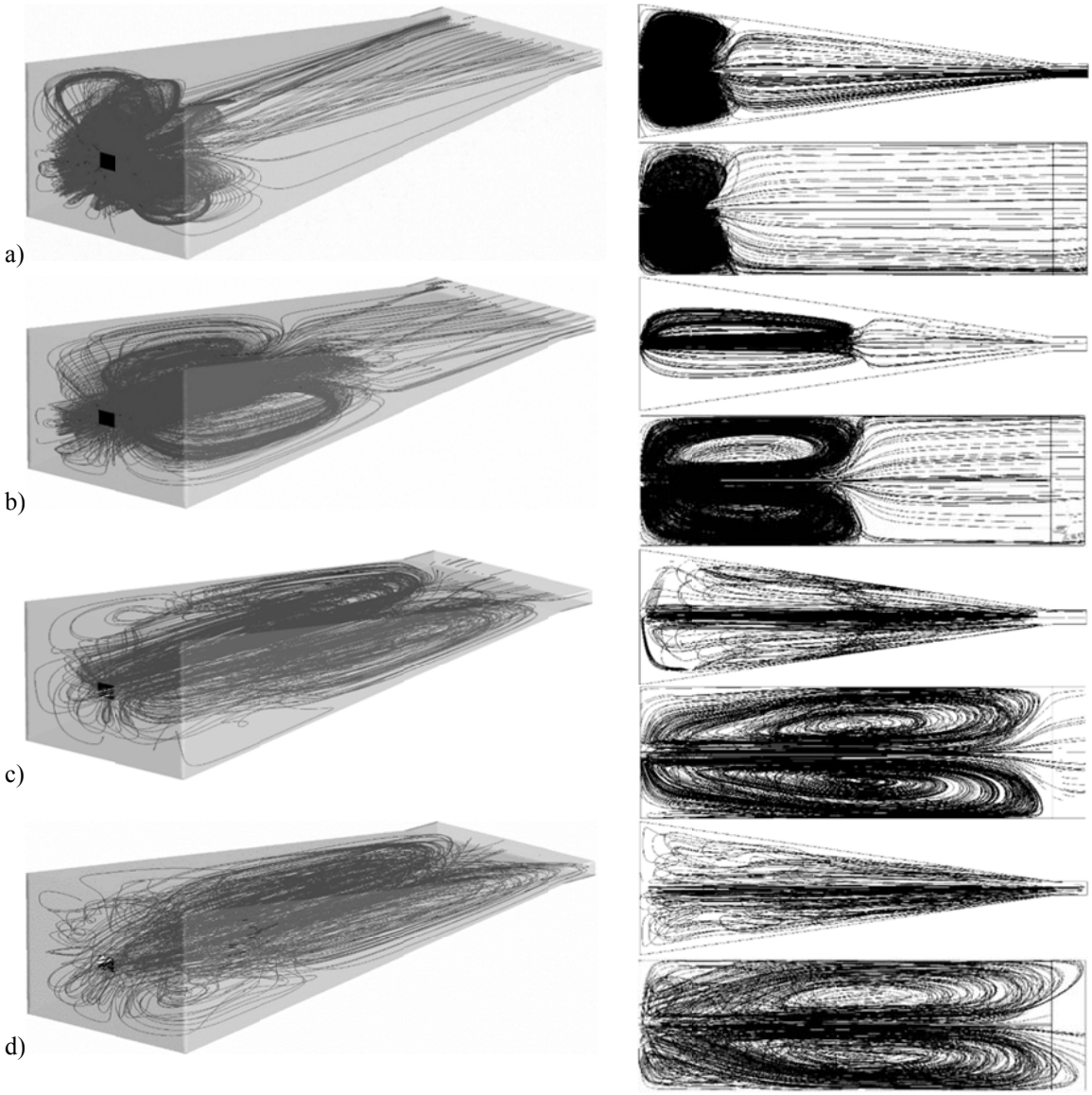


Fig. 9. Streamline contours for different Reynolds number at AR=10 and ϕ=0%. (a) Re=4000, (b) Re=10000, (c) Re=30000, (d) Re=40000

In Figure 10, the influence of aspect ratio on flow structure at Re=15,000 and ϕ=0% is shown. It is observed that for a low aspect ratio such as AR=2, the jet develops almost symmetric and back flow is seen immediately after the sudden expansion. The jet decay is rapid and the transition from jet-to-duct flow occurs in a short distance. At a higher aspect ratio of AR=20, it is observed that the steady state jet flow development is asymmetric. The transition from jet-to duct flow occurs over a longer distance as well. The main factor for this behavior is velocity difference between main flow at the center of channel and the part of flow that is close to the wall. With increasing aspect ratio velocity of jet flow enhance and velocity difference will be increased and recirculation zone extend.

In Figure 11, the influence of amplitude on flow structure at Re = 15000 is shown. It is observed that for low amplitude there isn't any recirculation zone in the dip of the wall. At higher amplitude of α= 0.04, it is observed that a recirculation zone formsin any wave of the sinusoidal wall. These zones have a great effect on increasing the local Nusselt number.

The effect of amplitude on Nusselt number is depicted in Figure 12. With increasing amplitude recirculation zones are formed in the dip of the wall. In addition chaotic behavior of the fluid flow will be increased and will have more impact between molecules of the fluid and the walls. These impacts cause more energy absorption by the fluid .These cause an average Nusselt number increase on both top and bottom walls.

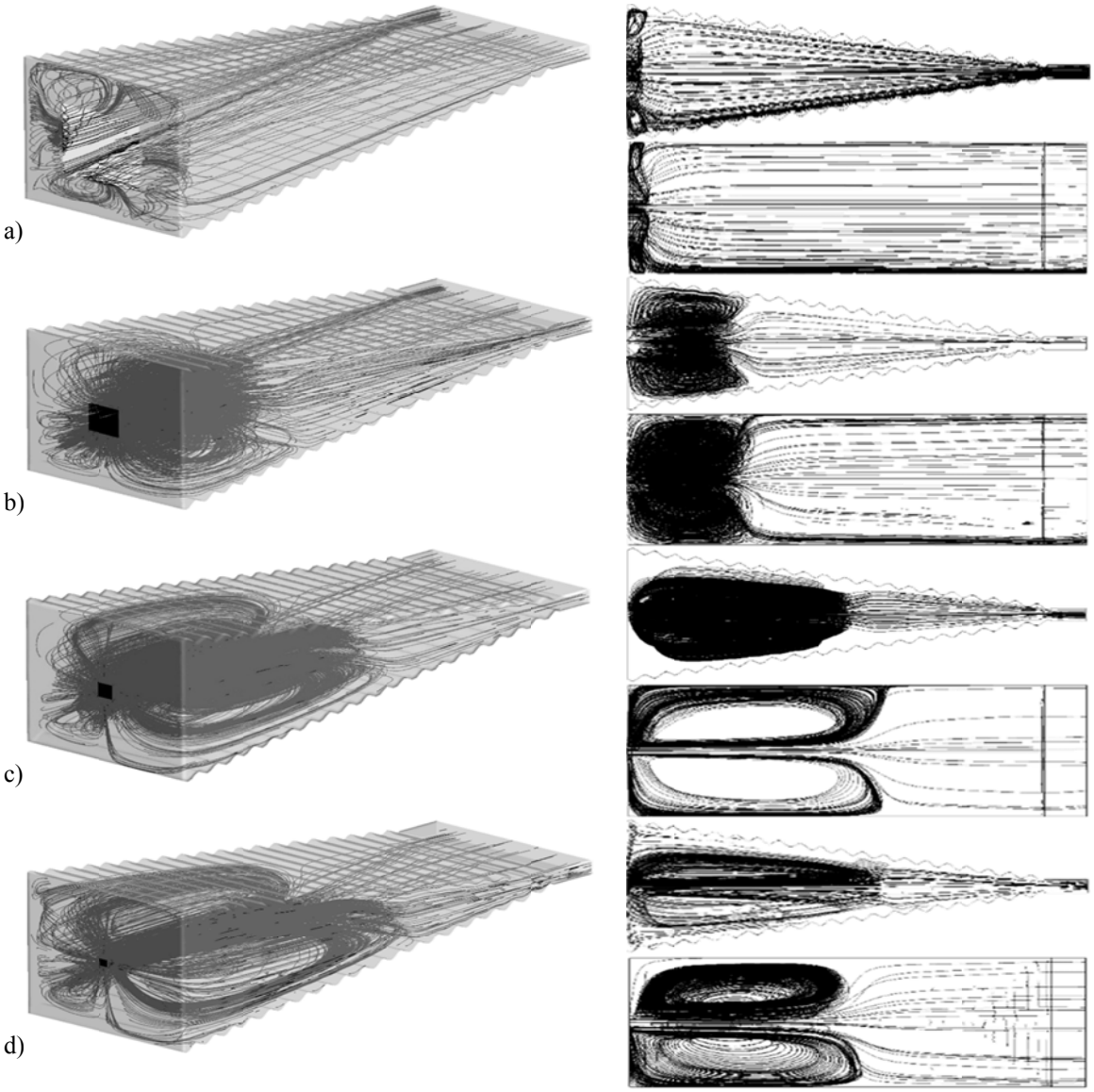


Fig. 10. Streamline contours for different aspect ratio at Re = 15000 and α= 0.02.(a) AR=2, (b) AR=5, (c) AR=10, (d) AR=20

Figure 13 shows the distribution of the Nusselt number at the top wall for Re = 10000 using different nanoparticles volume fractions. The figure reveals an enhancement in Nusselt number by increasing the volume fraction of nanoparticles. This behavior can be inferred from Equation 16. The effect of nanoparticles on the temperature difference term is negligible.

The effects of volume fraction of nanoparticles on the temperature gradient term and on the thermal conductivity ratio term are more pronounced. Before the point of reattachment as the volume fraction percentage of nanoparticles intensifies the temperature gradient at the top wall increases.

This is related to the addition inertia forces as depicted by Equation 4.

The equations show that any increase in volume fraction increases inertia forces becauseρ_{nf}will be increased and accordingly increases the temperature gradient. Besides, the nanoparticles increase the thermal conductivity ratio term as it can be seen from Equation 18. Therefore, both the temperature gradient term and thermal conductivity ratio term increase by increasing the volume fraction of nanoparticles. Accordingly, It can be seen that by increasing volume fraction the Nusselt number will be increased, because the heat transfer properties is improved.

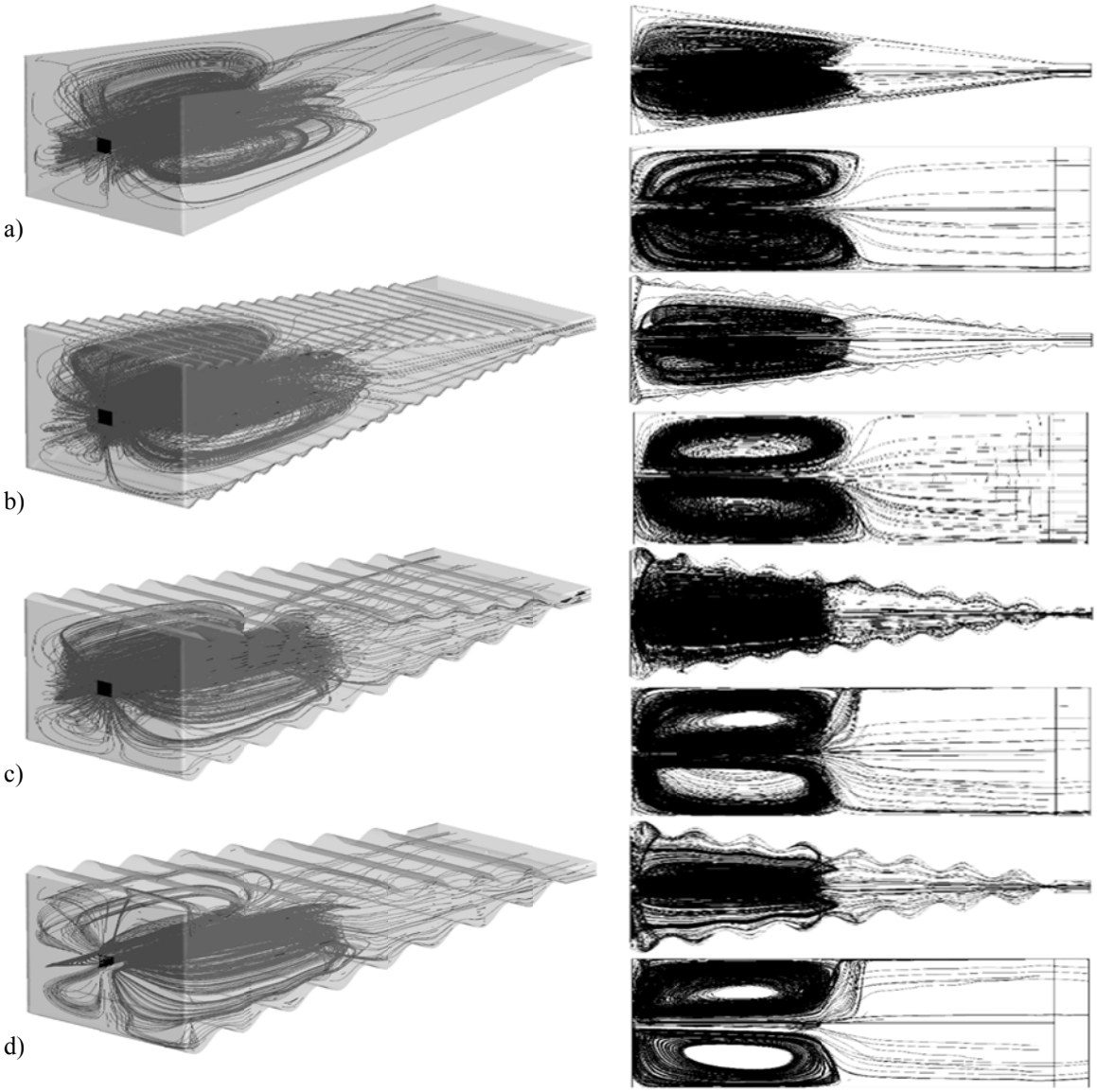


Fig. 11. Streamline contours for different amplitude at Re =10000 and AR =10.(a) α = 0, (b) α = 0.02, (c) α = 0.04, (d) α = 0.05

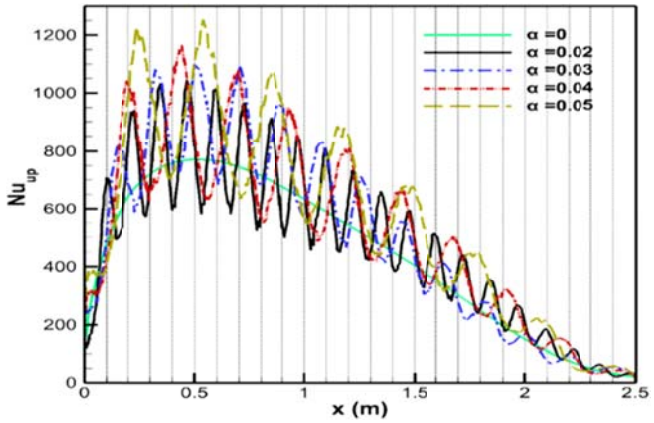


Fig. 12. Effect of amplitude on Nusselt number at AR=10, Re =10000

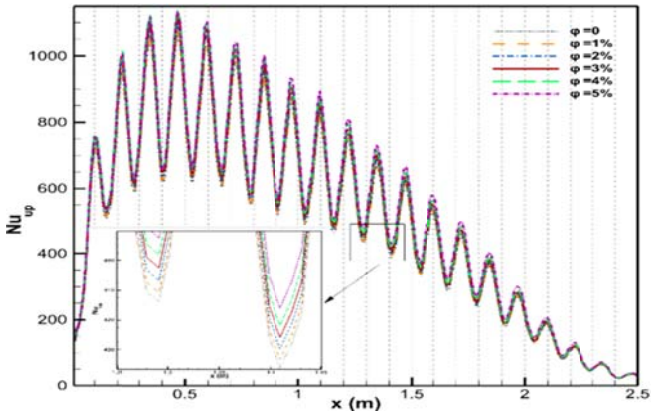


Fig. 13. Effect of nanopaticle's volume fraction on Nusselt number at Re =10000, α = 0.04, AR=10

CONCLUSION

In this paper, we reported the synthesis of maghemite nanoparticles by chemical precipitation route using ultrasonic radiation. Characterization of the obtained product morphology showed that nanoparticles are spherical, monodisperse and have an average core diameter of around 15 nm. The structural characterization of magnetic nanoparticles was further characterized through FTIR spectroscopy and XRD. The XRD pattern indicates that the γ-Fe_2O_3 product was well crystallized. The synthesized nanoparticles exhibited ferrimagnetic characteristics with the maximum saturation magnetization (MS) value of 68 emu/g.

The computational results showed that by increasing the Reynolds number, aspect ratio, volume fraction and amplitude the average Nusselt number will increase. The present computations reveal that when the volume fraction increases gradually from 0.0 to 0.05 the averaged Nusselt numbers will be increase 14 percent. Also 30 percent enhancement in averaged Nusselt number is seen by increasing amplitude from 0.0 to 0.04. It should be noted the intensification of turbulence eddy, suppression of the boundary layer, dispersion of the suspended particles, besides the augmentation of thermal conductivity and the heat capacity of the fluid were suggested to be the possible reasons for heat transfer enhancement.

ACKNOWLEDGMENT

The authors gratefully acknowledge the financial support of the Iranian Nanotechnology Initiative Council.

REFERENCES

[1] Oh JK, Park JM. Iron oxide-based superparamagnetic polymeric nanomaterials: design, preparation, and biomedical application. Progress in Polymer Science. 2011 Jan 31;36(1):168-89.

[2] Vala AK,Shah S.Rapid synthesis of silver nanoparticles by a marine-derived fungus Aspergillus niger and their antimicrobial potentials. International Journal of Nanoscience and Nanotechnology. 2012 Dec 30;8(4):197-206.

[3] Ragupathi C, Kennedy LJ, Vijaya JJ.A new approach :Synthesis, characterization and optical studies of nano-zinc aluminate. Advanced Powder Technology. 2014 Jan 31;25(1):267-73.

[4] Banerjee SS, Chen DH. Multifunctional pH-sensitive magnetic nanoparticles for simultaneous imaging, sensing and targeted intracellular anticancer drug delivery. Nanotechnology. 2008 Nov 24;19(50):505104.

[5] Karimi Z, Karimi L, Shokrollahi H. Nano-magnetic particles used in biomedicine: core and coating materials. Materials Science and Engineering: C. 2013 Jul 1;33(5):2465-75.

[6] Mir N, Nikkaran AR, Nejati-Yazdinejad M, Mir AA. Application of Magnetite Nanoparticles in Phenylalanine Removal from Water Samples. Journal of Nanostructures. 2013 Sep 1;3(3):341-6.

[7] Khayat Sarkar Z, Khayat Sarkar F. Selective removal of lead (II) ion from wastewater using superparamagnetic monodispersed iron oxide (Fe_3O_4) nanoparticles as a effective adsorbent. International Journal of Nanoscience and Nanotechnology. 2013 Jun 25;9(2):109-14.

[8] Strobel R, Pratsinis SE. Direct synthesis of magh - emite, magnetite and wustite nanoparticles by flame spray pyrolysis. Advanced Powder Technology. 2009 Mar 31;20(2):190-4.

[9] Chol SU. Enhancing thermal conductivity of fluids with nanoparticles. ASME-Publications-Fed. 1995 Nov 12;231:99-106.

[10] Ghalambaz M, Behseresht A, Behseresht J, Chamkha A. Effects of nanoparticles diameter and concentration on natural convection of the Al_2O_3–water nanofluids considering variable thermal conductivity around a vertical cone in porous media. Advanced Powder Technology. 2015 Jan 31;26(1):224-35.

[11] Safikhani H, Abbassi A. Effects of tube flattening on the fluid dynamic and heat transfer performance of nanofluids. Advanced Powder Technology. 2014 May 31;25(3):1132-41.

[12] Rahimi-Esbo M, Ranjbar AA, Ramiar A, Arya A, Rahgoshay M. Numerical study of turbulent forced convection jet flow in a converging sinusoidal channel. International Journal of Thermal Sciences. 2012 Sep 30;59:176-85.

[13] Esmaeili, E., R. Ghazanfari, and S. Farsad, Conv - ective heat transfer enhancement of the Water-based magnetite nanofluids in the presence of a 3-D low-intensity magnetic field. International Journal of Nano Dimension, 2014. 6(2): p. 141-151.

[14] Zeinali Heris S, Nassan TH, Noie SH. CuO/water nanofluid convective heat transfer through square duct under uniform heat flux. International Journal of Nanoscience and Nanotechnology. 2011 Sep 30;7(3):111-20.

[15] Takabi B, Shokouhmand H. Effects of Al_2O_3–Cu / water hybrid nanofluid on heat transfer and flow characteristics in turbulent regime. International Journal of Modern Physics C. 2015 Apr;26(04):1550047.

[16] Akbari OA, Toghraie D, Karimipour A. Impact of ri - bs on flow parameters and laminar heat transfer of water–aluminum oxide nanofluid with different nanoparticle volume fractions in a three-dimensional rectangular microchannel. Advances in Mechanical Engineering. 2015 Nov 24;7(11):168781401561815 5.

[17] Takabi B, Salehi S. Augmentation of the heat transfer performance of a sinusoidal corrugated enclosure by employing hybrid nanofluid. Advances in Mechanical Engineering. 2014 Mar 26;6:147059.

[18] Malvandi A, Ganji DD. Magnetic field and slip effects on free convection inside a vertical enclosure filled with alumina/water nanofluid. Chemical Engineering Research and Design. 2015 Feb 28;94:355-64.

[19] Vajjha RS , Das DK, Kulkarni DP. Development of new correlations for convective heat transfer and friction factor in turbulent regime for nanofluids. International Journal of Heat and Mass Transfer. 2010 Oct 31;53(21):4607-18.

[20] Rostamani M, Hosseinizadeh SF, Gorji M, Khodada- di JM. Numerical study of turbulent forced convection flow of nanofluids in a long horizontal duct considering variable properties. International Communications in Heat and Mass Transfer. 2010 Dec 31;37(10):1426-31.

[21] Chon CH, Kihm KD, Lee SP, Choi SU. Empirical correlation finding the role of temperature and particle size for nanofluid (Al_2O_3) thermal conductivity enhancement. Applied Physics Letters. 2005 Oct 10;87(15):153107.

[22] Mintsa HA, Roy G, Nguyen CT, Doucet D. New temperature dependent thermal conductivity data for water-based nanofluids. International Journal of Thermal Sciences. 2009 Feb 1;48(2):363-71.

[23] Masoumi N, Sohrabi N, Behzadmehr A.A new model for calculating the effective viscosity of nanofluids. Journal of Physics D: Applied Physics. 2009 Feb 9;42(5):055501.

[24] Pak BC, Cho YI. Hydrodynamic and heat transfer st- udy of dispersed fluids with submicron metallic oxide particles. Experimental Heat Transfer an International Journal. 1998 Apr 1;11(2):151-70.

[25] Pham, M. , F. Plourde, and S. Doan, Turbulent heat and mass transfer in sinusoidal wavy channels. International Journal of Heat and Fluid Flow, 2008. 29(5): p. 1240-1257.

[26] Zhang J, Muley A, Borghese JB, Manglik RM. Computational and experimental study of enhanced laminar flow heat transfer in three-dimensional sinusoidal wavy-plate-fin channels. InASME 2003 Heat Transfer Summer Conference 2003 Jan 1 (pp. 665-672). American Society of Mechanical Engineers.

[27] Inamdar, S.N. and S.K. Haram, Synthesis and Characterization of Uncapped Fe_2O_3 Nanoparticles Prepared by Flame Pyrolysis of Ferrocene in Ethanol. Journal of nanoscience and nanotechnology, 2006. 6(7): p. 2155-2158.

[28] Darezereshki, E., Synthesis of maghemite Fe_2O_3 nanoparticles by wet chemical method at room temperature. Materials Letters, 2010. 64(13): p. 1471-1472.

[29] Chakrabarti S, Ganguli D, Chaudhuri S. Optical properties of γ-Fe_2O_3 nanoparticles dispersed on sol–gel silica spheres. Physica E: Low-dimensional Systems and Nanostructures. 2004 Sep 30;24(3):333-42.

[30] Cao SW, Zhu YJ, Ma MY, Li L, Zhang L. Hierarchically nanostructured magnetic hollow spheres of Fe_3O_4 and γ-Fe_2O_3: preparation and potential application in drug delivery. The Journal of Physical Chemistry C. 2008 Feb 14;112(6):1851-6.

[31] Sarma AS, Sundararajan T, Ramjee V. Numerical simulation of confined laminar jet flows. International journal for numerical methods in fluids. 2000 Jul 15;33(5):609-26.